Angewandte Chemie
Eine Zeitschrift der Gesellschaft Deutscher Chemiker

Supporting Information

Thermally Stable and Regenerable Platinum–Tin Clusters for Propane Dehydrogenation Prepared by Atom Trapping on Ceria

Haifeng Xiong, Sen Lin, Joris Goetze, Paul Pletcher, Hua Guo, Libor Kovarik, Kateryna Artyushkova, Bert M. Weckhuysen,* and Abhaya K. Datye**

anie_201701115_sm_miscellaneous_information.pdf

Supporting Information

This PDF file includes:
Materials and Methods
Supplementary Text
Supplementary Figures S1 to S19
Supplementary Tables S1 to S5

Materials and Methods

Catalyst preparation CeO_2 was prepared by calcining cerium nitrate (Sigma Aldrich) at 350 ^oC for 4 h. Sn-doped CeO_2 with a Sn loading of 3 wt.% (Sn-CeO_2) was prepared by impregnating $SnCl_4$ solution into the aforementioned CeO_2, followed by calcining at 500 ^oC for 6 h in air. γ-Al_2O_3 was prepared by calcining the aluminum oxide (Sasol, PURAL 400) at 900 ^oC for 24 h in air. Sn-doped Al_2O_3 with Sn loading of 3 wt.% (Sn-Al_2O_3) was prepared by impregnating $SnCl_4$ solution into the aforementioned Al_2O_3, followed by calcining at 500 ^oC for 6 h in air. Pt catalyst supported on CeO_2, Sn-CeO_2 and Sn-Al_2O_3 were prepared by incipient wetness impregnation. Briefly, appropriate amount of chloroplatinic acid (Sigma Aldrich, 8wt.%) was added dropwise to the supports. The mixture was dried at 100 ^oC for 12 h. The Pt/CeO_2 and Pt-Sn/CeO_2 catalysts were calcined at 800 ^oC for 10 h in flowing air. The Pt-Sn/Al_2O_3 was calcined at 550 ^oC for 6 h in a flow of air. In order to subject the catalyst to severe sintering under reducing conditions, we also treated the Pt-Sn/CeO_2 catalyst containing atomically-dispersed Pt in flowing CH_4 (100 mL/min) at 800 ^oC for 30 min. The temperature was then decreased to 500 ^oC and the sample was treated in air at 500 ^oC for 1 h to remove the surface carbon.

Catalyst Characterization

The surface area of the samples was measured using a Micromeritics Gemini 2360 surface area analyzer by the multi-point BET method using N_2 adsorption at -196 ˚C. Scanning transmission electron microscopy was partly carried out using a JEOL 2010F 200kV transmission electron microscope (resolution of 0.14 nm). The powders were deposited on holey carbon support films after being dispersed in ethanol. For atomic resolution imaging, we used a JEOL JEM ARMS200CF 200 kV aberration-corrected (AC) transmission electron microscope (resolution of 0.08 nm). Part of the high-resolution STEM imaging was performed with a FEI Titan 80-300 microscope operated at 300 kV. The instrument is equipped with a CEOS GmbH double-hexapole aberration corrector for the probe-forming lens, which allows imaging with 0.1 nm resolution in scanning transmission electron microscopy (STEM) mode. The STEM images were acquired in the high angle annular dark field (HAADF) image mode with an inner collection angle of 52 mrad. The elemental analysis was performed using an EDAX Si (Li) EDS detector and FEI TIA analysis software. The Pt single atoms and clusters on CeO_2-based catalysts can be clearly seen in the aberration corrected (AC) STEM dark field images. X-ray photoelectron spectroscopy (XPS) was performed using a Kratos Axis Ultra photoelectron spectrometer equipped with a monochromatic Al Kα source operating at 300 W. The base pressure was 2.7×10^{-8} Pa, and operating pressure was 2.7×10^{-7} Pa. XPS was performed in order to study the chemical state of Pt catalyst before and after dehydrogenation. Analysis of the XPS spectra was performed using CASA XPS software. Both thermogravimetric analysis (TGA) and CHN elemental analysis were used to measure the coke content of the spent catalysts. TGA was performed using a TA Instruments SDT Q600 TGA/DSC that can heat at temperatures ranging from 25 °C to 1000 °C. TGA was used to determine the coke loading on the spent Pt catalysts after dehydrogenation in flowing air. CHN elemental analysis was carried out using a Costech ECS 4010 Elemental Analyzer coupled to a Thermo Finnigan Delta V Advantage Plus mass spectrometer via a CONFLO II interface. CO diffuse reflectance infrared Fourier transform spectroscopy (DRIFTS) and TPD experiments were conducted using a Harrick Praying Mantis High accessory fitted with ZnSe windows. FTIR measurements were taken using a Tensor 37 Bruker spectrometer with a liquid nitrogen cooled MCT detector. The background for the measurements was taken with KBr. High purity He, CO, and H_2 were purchased from Linde. These gases were used without further purification. The procedure for the CO TPD experiments was as follows. The catalyst in the cell was equilibrated to room temperature under gas flow for 20 min. Depending on the experiment, a 20 mL/min He or H_2 gas flow was used. The sample was heated to 300 °C at 3 °C/min and kept there for 1 h. After that, the cell was cooled to 30 °C in a 20 mL/min flow of He. CO dosing occurred under a flow rate of 5 mL/min CO and 5 mL/min He. After 30 min, the CO gas flow was turned off and the He gas flow was

increased to 20 mL/min to flush the cell for 30 min. Spectra were then recorded. The CO TPD experiment was carried out by heating the sample from 30 °C to 300 °C at 3 °C/min. Spectra were taken every 10 °C.

Reaction measurements

Propane dehydrogenation at UNM was carried out in a down-flow packed bed reactor. The reactor consists of a cylindrical quartz tube (ID=10 mm), which is placed inside an oven (ATS, Applied Test System). Inside the tube, 0.1 g of catalyst powder is loaded on top of a bed of quartz wool. The experiments were described briefly as follows: a carrier gas was firstly introduced to the reactor with a flowrate of 10 mL/min for 30 min and then, the temperature was increased to 680 ºC with a rate of 10 ºC/min in the flowing of carrier gas. After that, C_3H_8 was introduced to the reactor with a flowrate of 2 mL/min. In addition, liquid water was pumped to the reactor (0.005 ml/min) and the water line was always kept at 160 ºC. After the reactor, we added a stream of 50 ml/min of Ar to dilute the products so as to bring the concentrations to a suitable range for detection by the GC. The analysis is performed by a VARIAN CP-3800 GC, equipped with a flame ionization detector and a thermal conductivity detector to study the composition of the reactor stream. The former detector is used to quantify the flammable gases in the product stream (with the exception of hydrogen), which are CH_4, C_2H_4, C_2H_6, C_3H_6 and C_3H_8. The latter detector is used to quantify the other gases present in the system based on thermal conductivity: H_2 and hydrocarbons, CO and CO_2. However, because of the diluted reactor effluent, we were not able to quantify the products detected by the TCD. For this reason, we performed additional experiments using a reactor system at Utrecht University, which are described later. For multi-cycle experiments, the spent catalyst (after reaction) was subjected to an oxidative regeneration step after 6 h on stream. This involved treating the sample in flowing air at 580 ºC for 2 h.

To confirm the catalytic results obtained at UNM, similar experiments were performed at Utrecht University at reaction temperatures of 550 and 680 ºC. In a rectangular quartz tube reactor (ID = 3 mm × 6 mm), 0.1 g catalyst was loaded. C_3H_8 with a flowrate of 2 mL/min was mixed with He (10 ml/min) and introduced into the reactor. Liquid water was introduced into the gas stream using a saturator at a rate of 1.6 mg/min. All gas lines were heat traced to 200 ºC. Online analysis of the reactant and reaction products was performed using an Interscience Compact GC, equipped with an Rtx-wax and Rtx-1 column in series and an Rtx-1, Rt-TCEP and Al_2O_3/Na_2SO_4 in series, both connected to an FID detector. The propane conversion (X) and propylene selectivity (S) was calculated based on the following formulas:

$$X = \frac{moles\ of\ propane\ inlet - moles\ of\ propane\ outlet}{moles\ of\ propane\ inlet} \times 100\%$$

$$S = \frac{moles\ of\ propylene}{moles\ of\ propylene + moles\ of\ CH4/3 + 2 * moles\ of\ C2\ hydrocarbons/3} \times 100\%$$

At UNM, since we performed analysis using a diluted effluent (2mL/min propane+50 mL/min inert+3 mL/min water vapor), we can ignore the change of moles during reaction and assume the volumetric flow rate remains the same. The moles of propane can therefore be obtained from the GC peak areas, which are proportional to the concentration of propane.

At Utrecht, the analysis included all of the products. The increase in volume during the reaction was calculated based on the amount of H_2 produced during the reaction. Hence, we are able to report the carbon balance and the total carbon selectivity for each of the products as shown below for propylene:

$$S = \frac{moles\ of\ propylene \times 100}{moles\ of\ propylene + \frac{moles\ of\ CH4}{3} + \frac{2 * moles\ of\ C2\ hydrocarbons}{3} + \frac{moles\ of\ CO}{3} + \frac{moles\ of\ CO2}{3}}$$

DFT calculations

All spin-polarized density functional theory (DFT) calculations were carried out in Vienna *ab initio* simulation package (VASP) [1, 2] with the gradient-corrected PW91 exchange-correction functional.[3] The electronic wave functions are expanded in plane waves up to a cutoff energy of 9224.02 kcal/mol and the ionic core-electron interaction is approximated by the projector augmented-wave (PAW) method.[4] For CeO_2, a strongly correlated system, it is a necessary requirement to correct the incomplete cancellation of the self-interaction error in the generalized gradient approximation (GGA). In this work, in order to properly describe the behavior of electrons occupying the f orbitals of Ce in CeO_2, DFT + U with U = 92.24 kcal/mol was used.[5, 6] The optimized bulk lattice parameter for CeO_2 was found to be 5.42 Å, in good agreement with the experimental value (5.41 Å) [7]. Our slab model of the CeO_2(111) contains a 2×2 surface unit cell with a total of nine atomic layers. The top six atomic layers were relaxed during optimization, while the bottom three layers were fixed. A vacuum space of 14 Å is employed between the neighboring interleaved slabs. To sample the Brillouin zone, a 2×2×1 Monkhorst-Pack *k*-point grids[8] were adopted, which is tested to be converged. The adsorption energy of a pertinent species is computed as follows: $E_{ads} = E_{(adsorbate + surface)} - E_{(free\ molecule)} - E_{(free\ surface)}$. The transition states (TSs) between initial states (ISs) and final states (FSs) were determined using the climb image nudged elastic band (NEB) method.[9] The convergence of relaxation was checked with the 1.15 kcal/mol/Å criterion. The total energy difference is less than 2.31×10^{-3} kcal/mol.

Discussion of DFT results

As shown in Figure S3, the doped Sn occupies a surface Ce site and form strong interactions with the neighboring oxygens without significant distorting the lattice. The adsorption energy of Sn at the Ce site is -304.54 kcal/mol. As displayed in Figure S3, a Pt atom readily adsorb at the Sn site, with an adsorption energy of 101.85 kcal/mol. This Pt atom is much more stable than its adsorption on the (111) face of CeO_2, which has an adsorption energy of 66.67 kcal/mol. In order to investigate the formation of nanoclusters, we computed the adsorption energy of an additional Pt atom for both cases (Figure S3c). For Pt/CeO_2, the adsorption energy for an additional Pt is 89.16 kcal/mol, which is slightly larger than (75.72 kcal/mol) that for Pt-Sn/CeO_2. However, since the latter is more strongly bound, the clustering is more likely to occur near the Sn site. Thus, the Sn is capable of acting as a nucleation site for the growth of single Pt atoms to generate Pt clusters, which is in agreement with our STEM results. This is consistent with our STEM-EDS results (Pt/Sn atomic ratio > 1 for the Pt-Sn clusters, Figure S7)

The Bader charge calculations suggest that the Pt atom on the CeO_2 without Sn-doping is positively charged with a value of +0.15 |e|. When Sn is doped into the Ce site, the calculated charge on Sn is about +2.19 |e|. While the Pt is located at the Sn-CeO_2 site, the charge on Sn is reduced to +1.97 |e| and Pt possess more positive charge of +0.30 |e|. This observation is confirmed by the differential charge density calculations (Figure S3d) that electrons transfer from Pt to Sn.

The reaction paths for propane dehydrogenation to propylene have been investigated on both the Pt/CeO_2 and Pt-Sn/CeO_2 surfaces. On Pt/CeO_2, and the configurations for the ISs, TSs, and FSs of reaction paths for $CH_3CH_2H_3^* \rightarrow CH_3CH_2CH_2^* + H^*$ and $CH_3CH_2CH_2^* \rightarrow CH_3CHCH_2^* + H^*$ on the Pt atoms in the Pt-Sn/CeO_2 catalyst are shown in Figure S5. Note that the second dehydrogenation step involves two TSs. The barriers and reaction energies are listed in Table S2. The low barriers in this process are consistent with the high reactivity observed in experiment. Interestingly, the propylene product is strongly bond to the Pt in this case. Similarly, the configurations for the ISs, TSs, and FSs of the same reaction steps on the Pt-Sn cluster (Pt/Sn atomic ratio=1) supported on CeO_2 are shown in Figure S17. Comparing with the Pt/CeO_2 catalyst, the dehydrogenation steps require much higher activation energies for the Pt-Sn/CeO_2 catalyst, However, the targeted product (propylene) adsorbs weakly at the Pt atoms on the Pt-Sn/CeO_2 catalyst. This is reminiscent of the adsorption pattern in the dehydrogenation of propane on Pt-Sn alloys, where the weak

adsorption of propylene is identified as the key factor for its selectivity [10, 11]. A key observation is that although the reaction steps are much more highly activated at the Pt-Sn/CeO_2 site than those at the Pt/CeO_2 site, the product propylene at the former site has a much lower adsorption energy. For this reason, propylene is much less likely to be available on the Pt-Sn/CeO_2 catalyst for further dehydrogenation, which might eventually lead to methane and coke formation on the catalyst [12]. This is consistent with the experimental observation reported here that the dehydrogenation of propane has a lower reactivity but much higher selectivity towards propylene on the Pt-Sn/CeO_2 catalyst. We have also investigated the dehydrogenation on a Pt-Sn cluster (Pt/Sn atomic ratio=2) on CeO_2 (Figure S3c). However, similar to the single atom Pt/CeO_2 catalyst, the Pt-Sn cluster on CeO_2 with a Pt/Sn ratio of 2 shows high propylene adsorption energy. This indicates that this Pt-Sn cluster catalyst is less selective than the Pt-Sn/CeO_2 catalyst with Pt/Sn ratio of 1, which agrees well with our experiment result that the as-prepared Pt-Sn cluster is less selective in the first 2 h run of propane dehydrogenation (Fig. 2d).

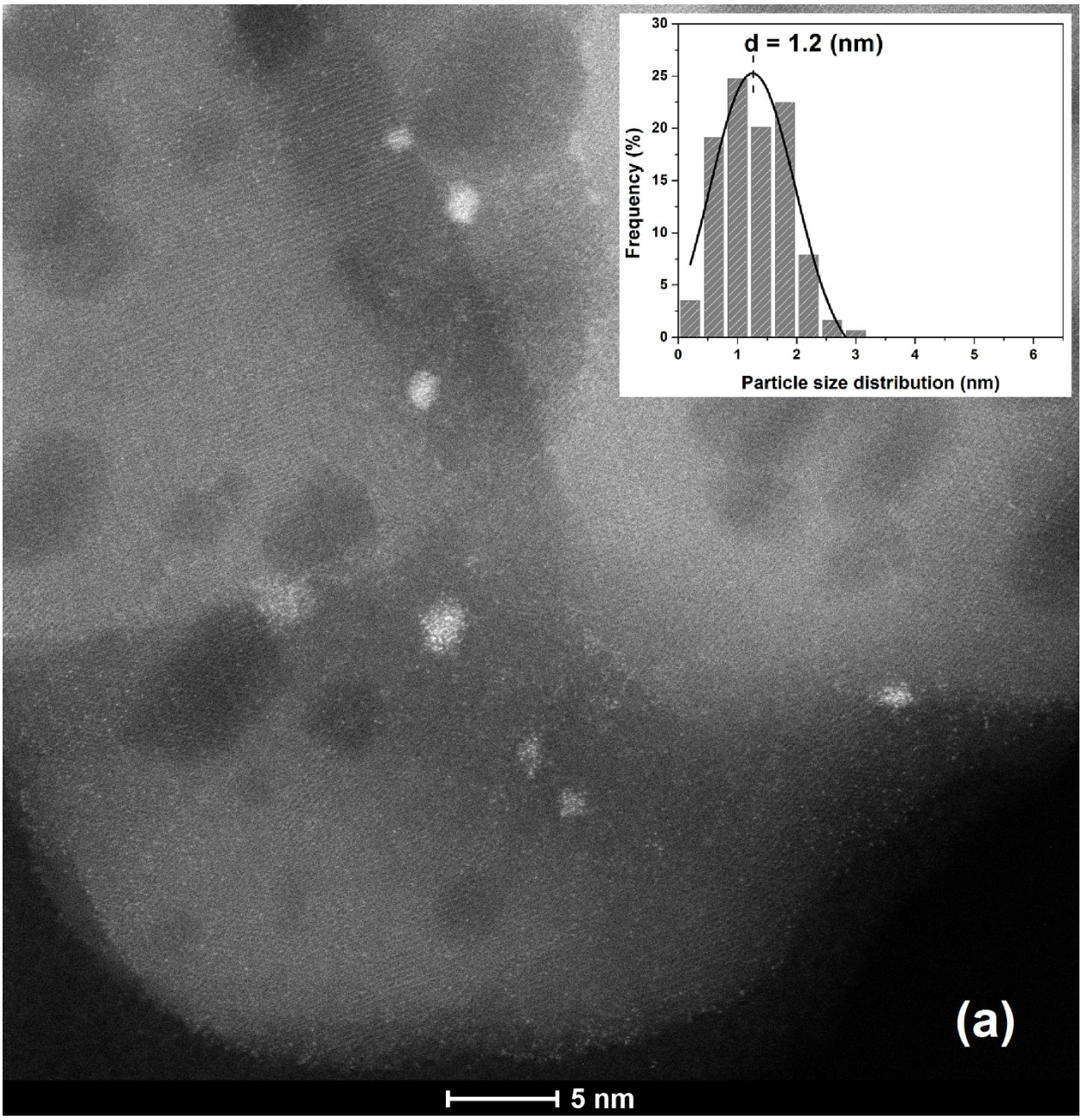
d = 1.2 (nm)
Frequency (%)
Particle size distribution (nm)
(a)
5 nm

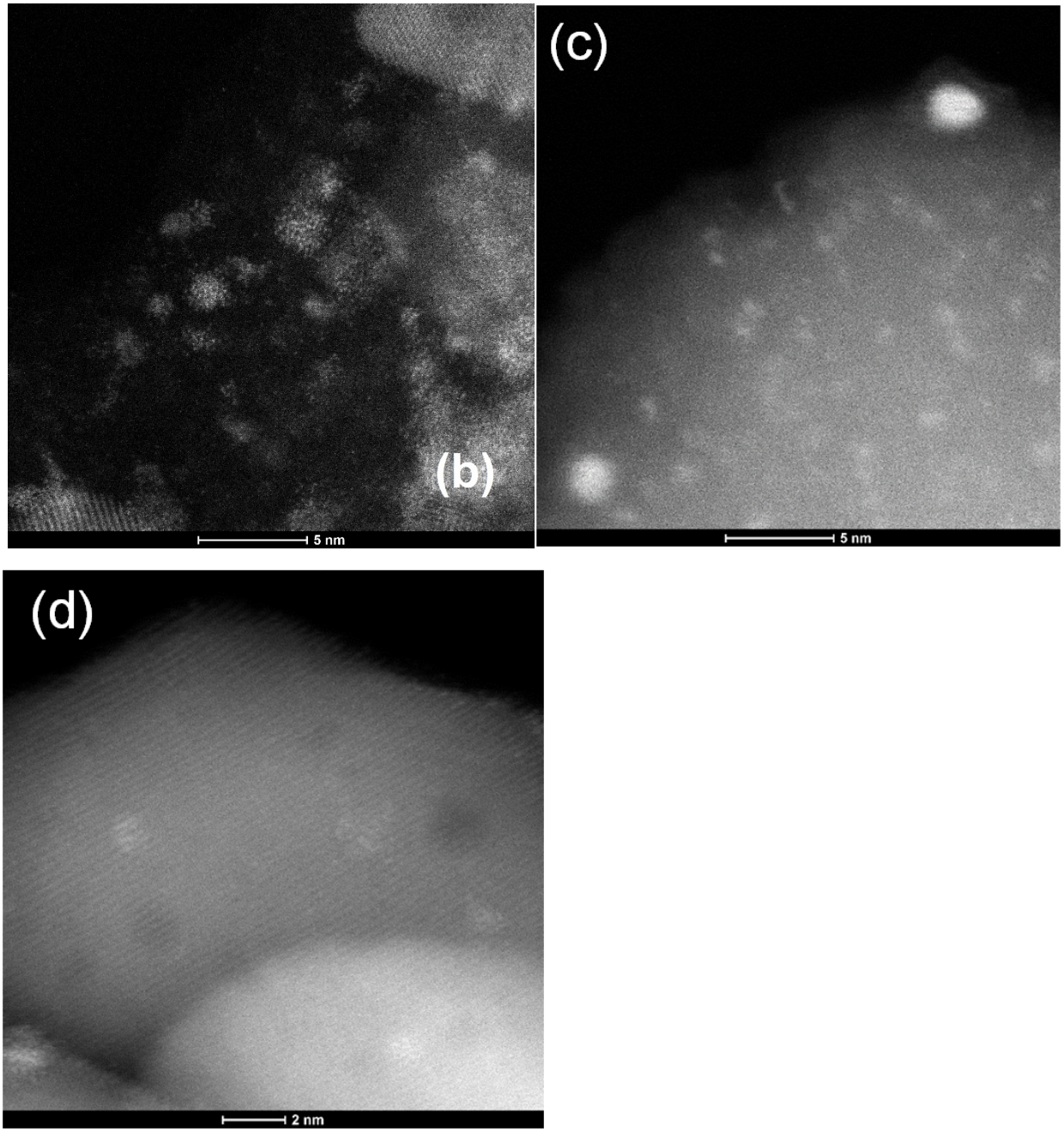

Supplementary Figure S1. STEM images of (a and b) Pt/CeO_2 and (c and d) $Pt\text{-}Sn/CeO_2$ catalysts after three cycles of propane dehydrogenation at 680 ^oC (each cycle was carried out for 6 h). The inset in (a) shows the Pt cluster size distribution on the spent Pt/CeO_2. The spent Pt/CeO_2 shows single atoms co-existing with sub-nanometer particles. The spent $Pt\text{-}Sn/CeO_2$ only shows clusters.

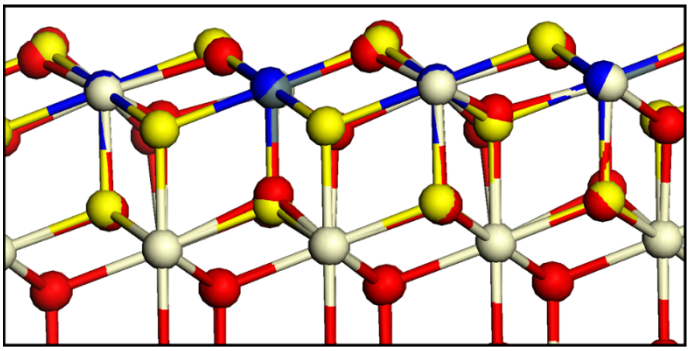

Supplementary Figure S2. Configurational reconstruction of CeO_2 after Sn replacing a lattice Ce. Color scheme: Ce, yellow; O, red; Sn, grey (different colors are used if positions are changed).

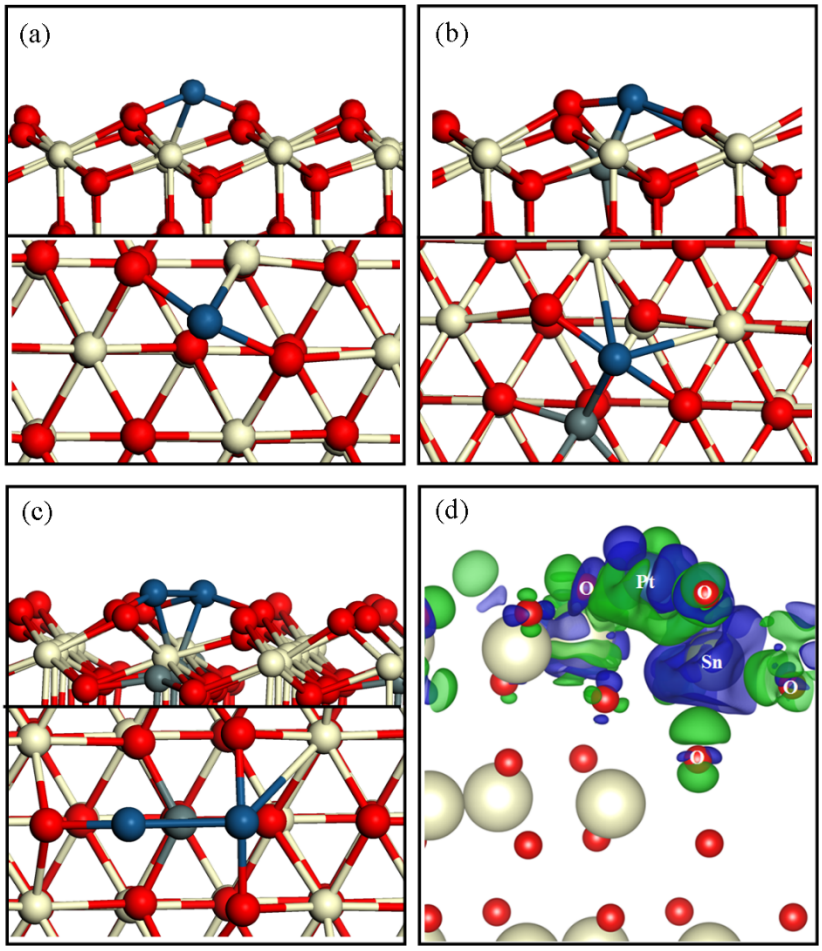

Supplementary Figure S3. Top and side views for the geometries of (a) Pt/CeO_2, (b) $Pt\text{-}Sn/CeO_2$, (c) a second Pt adsorption on $Pt\text{-}Sn/CeO_2$ (111) and (d) Contour plot of differential charge density of $Pt\text{-}Sn/CeO_2$. The accumulation region is rendered in blue, and the charge depletion region is in green (the isovalue is 0.007 au). Color scheme: Ce, yellow; O, red; Pt, blue; Sn, grey.

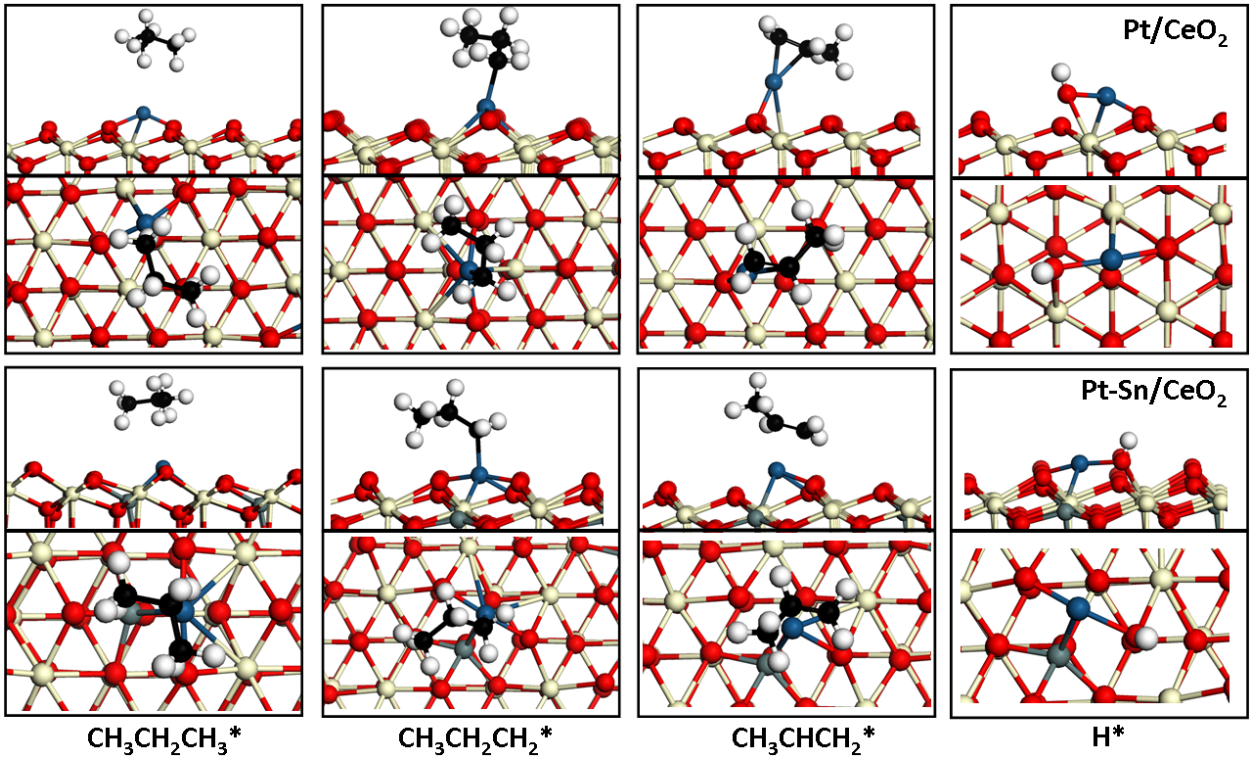

Supplementary Figure S4. The configurations of relevant species adsorption on Pt/CeO_2 and $Pt\text{-}Sn/CeO_2$, respectively. Color scheme: Ce, yellow; O, red; Pt, blue; Sn, grey; C, black; H, white.

Table S1

Calculated adsorption energies of relevant species on CeO_2, Pt/CeO_2 and $Pt\text{-}Sn/CeO_2$

	Pt/CeO_2 (eV)	$Pt\text{-}Sn/CeO_2$ (eV)
Pt	-2.89	-4.42
$CH_3CH_2CH_3$	-0.70	-0.04
$CH_3CH_2CH_2$	-2.01	-2.16
CH_3CHCH_2	-2.21	-0.69
H on the top of Pt	-2.53	-2.39
H on the top of lattice O1	-2.87	-2.94
H on the top of lattice O2	-3.08	-3.00

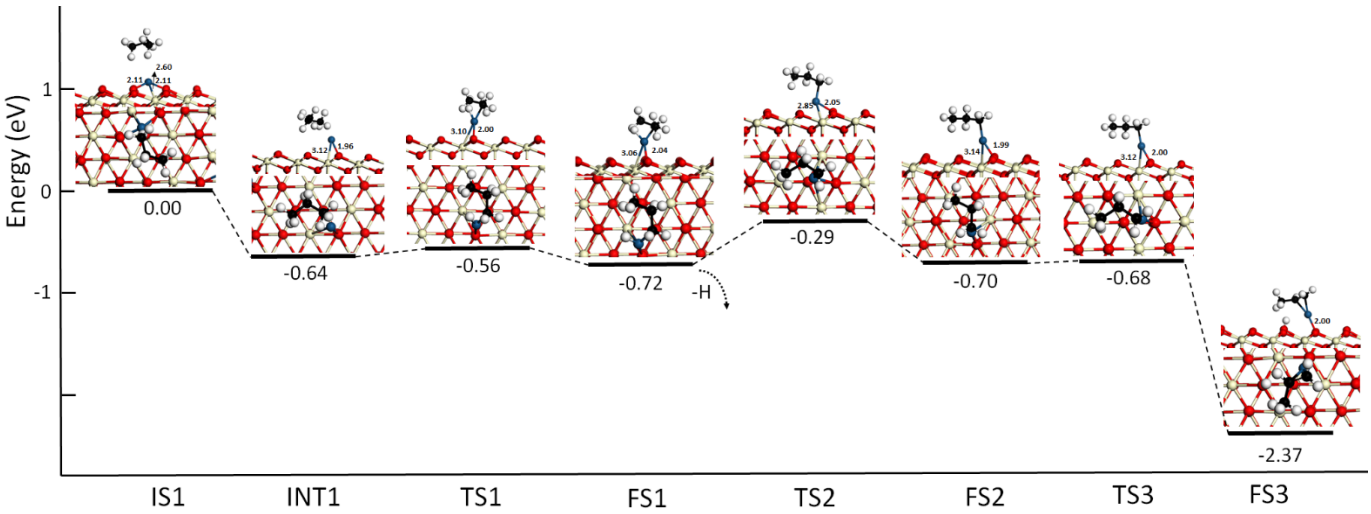

Supplementary Figure S5. The calculated reaction paths for $CH_3CH_2CH_3$* → $CH_3CH_2CH_2$* + H* and $CH_3CH_2CH_2$*→ CH_3CHCH_2*+ H* on Pt/CeO_2. Color scheme: Ce, yellow; O, red; Pt, blue; C, black; H, white.

Table S2

Calculated activation energy (E_a)/reaction energies (ΔE) (eV) for $CH_3CH_2H_3^*$ → $CH_3CH_2CH_2^*$ + H* and $CH_3CH_2CH_2^*$→ $CH_3CHCH_2^*$+ H* on Pt/CeO_2 and $Pt\text{-}Sn/CeO_2$, respectively.

	Pt/CeO_2		$Pt\text{-}Sn/CeO_2$
	Step1	Step2	
$CH_3CH_2H_3^*$ → $CH_3CH_2CH_2^*$ + H*	0/-0.64	0.08/-0.08	0.60/-0.33
$CH_3CH_2CH_2^*$→ $CH_3CHCH_2^*$+ H*	0.43/0.02	0.02/-1.67	1.37/-0.18

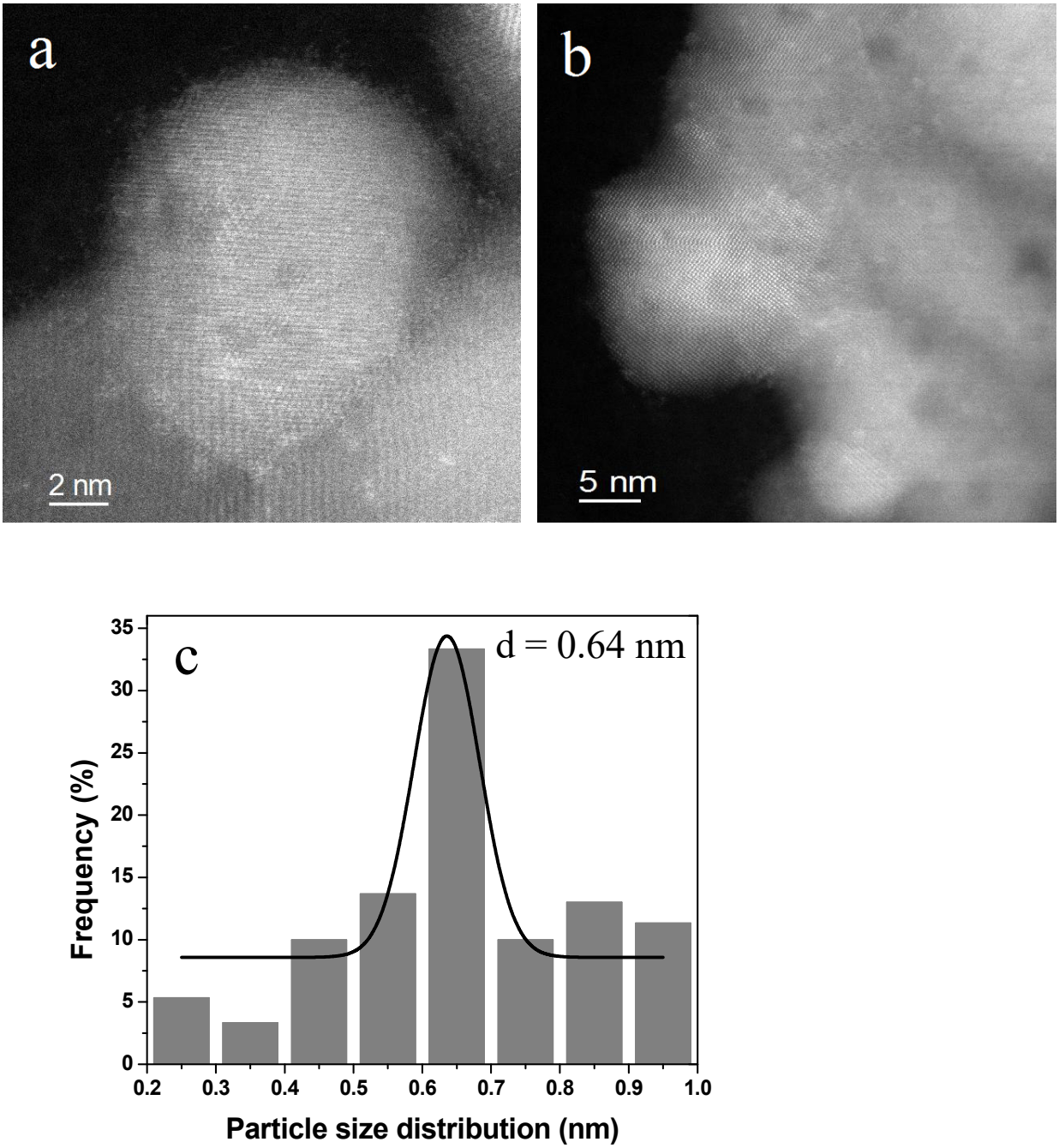

Supplementary Figure S6. (a) and (b) STEM images of Pt-Sn/CeO_2 catalyst as prepared after 800 ^oC calcination in air showing atomically dispersed species and also sub-nanometer particles on CeO_2; (c) the cluster size distribution of Pt-Sn/CeO_2 catalyst showing that the clusters are smaller than 1 nm.

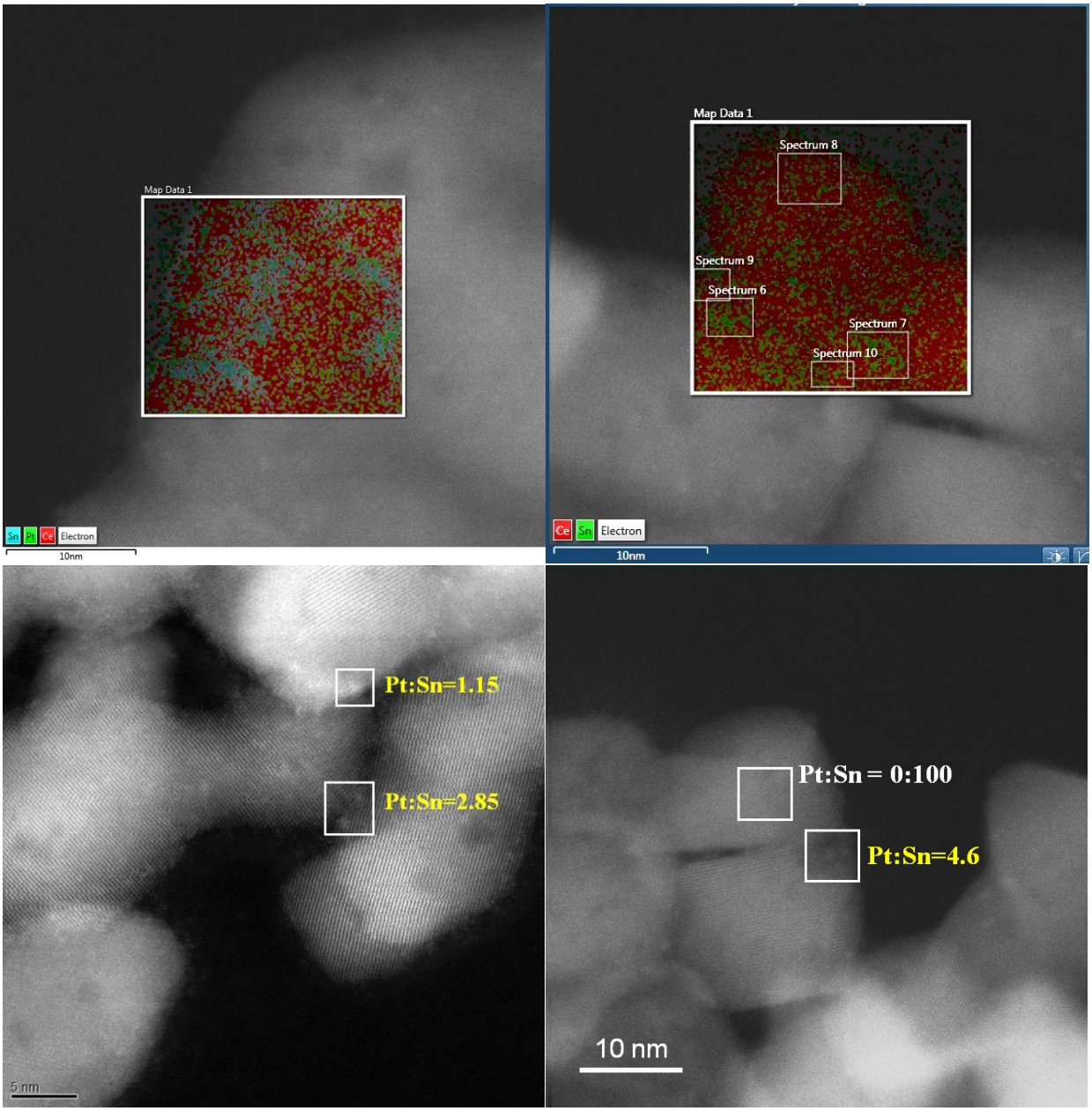

Supplementary Figure S7. STEM-EDS analysis of Pt-Sn/CeO_2 catalyst as prepared after 800 ºC calcination in air showing sub-nm clusters, which contain Pt and Sn with an atomic ratio of Pt:Sn in the range from 1:1 to 5:1.

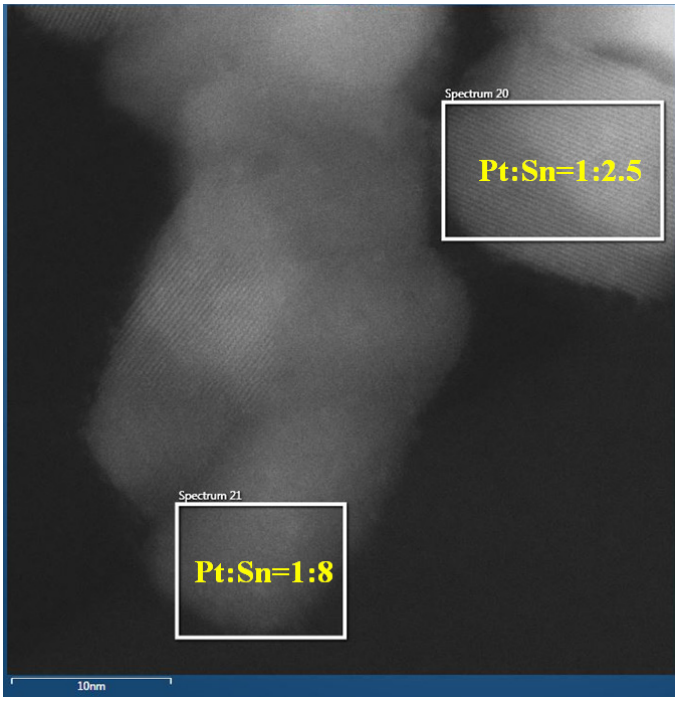

Supplementary Figure S8. STEM-EDS analysis of Pt-Sn/CeO_2 catalyst as prepared after 800 ^oC calcination in air at regions which do not contain detectable sub-nm clusters. These regions show a high Sn content, but the Sn atoms cannot be imaged because of poor atomic number contrast (Sn atomic number: 50; Ce atomic number: 58; Pt atomic number: 78). The atomic ratio of Sn to Pt ranges from 100:1 to 2.5:1.

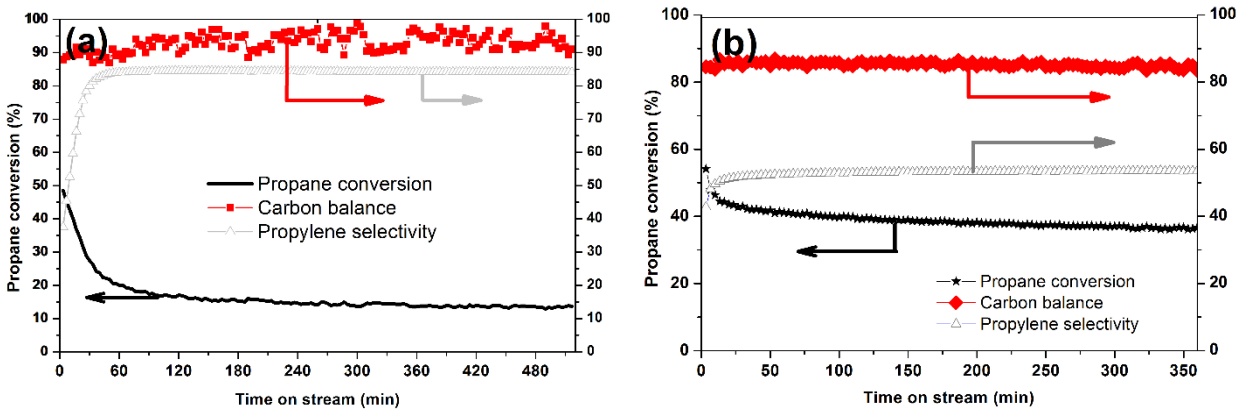

Supplementary Figure S9. Propane dehydrogenation reactivity of Pt-Sn/CeO_2 catalyst using the reactor system at Utrecht. The measurements were conducted at (a) 550 °C and (b) 680 ºC using a lower content of water, compared to the UNM experiments (C_3H_8 flowrate: 2 mL/min, carrier gas flowrate (He): 10 mL/min; liquid water flowrate: 0.0016 mL/min).

Table S3

Product selectivity for the reactivity measurements reported in Figure S9. The initial catalyst shows very different behavior but after the period of self-assembly the catalyst achieves improved selectivity which is stable through the end of the run.

Time on stream	Product selectivity (expressed as % carbon in each product)											
	550 °C						680 °C					
	C_3H_6	CH_4	CO	CO_2	C_2H_4	C_2H_6	C_3H_6	CH_4	CO	CO_2	C_2H_4	C_2H_6
initial	37.5	9.6	13.6	13.9	1.6	23.7	43.5	16.1	17.7	12.8	3.4	6.3
2 h (after self assembly)	84.5	4.6	0.4	6.0	2.9	1.4	53.8	13.6	5.18	13.1	2.2	12.1
End of run	84.1	4.9	0.35	5.4	4.1	1.2	54.2	13.6	3.6	12.0	1.9	14.5

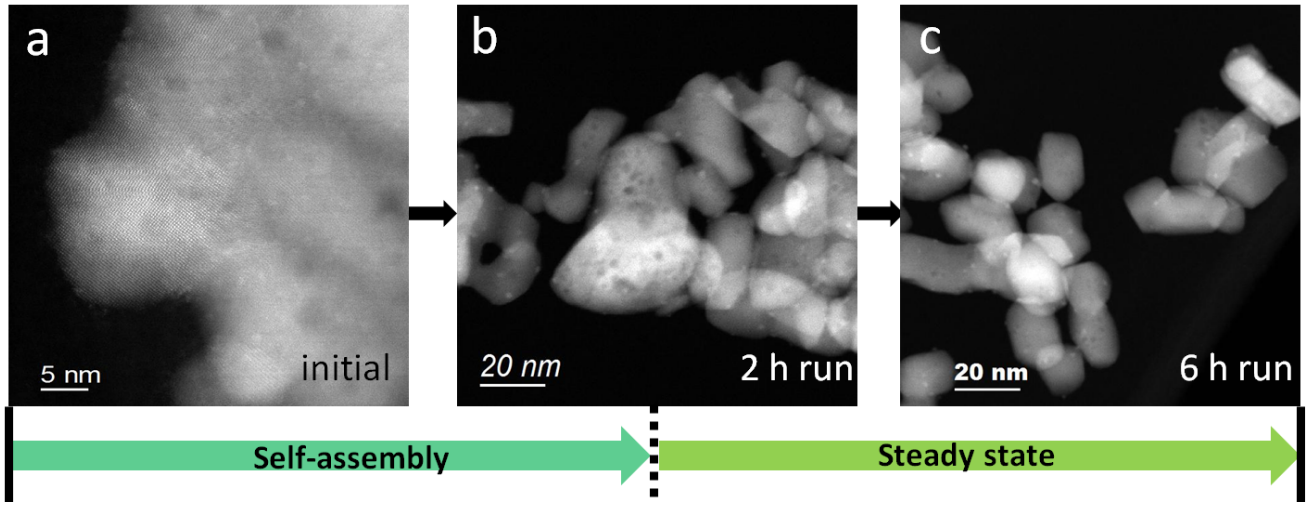

Supplementary Figure S10. STEM images of the Pt-Sn/CeO_2 show the comparison of the catalyst at the initial "as-prepared" state, after 2 h run and after 6 h. The initial "as-prepared" sample shows atomically dispersed Pt with some nanoclusters. After 2 h, we see well-defined nanoparticles indicating that the process of self-assembly is complete. After 6 h, we see a very similar particle size distribution, which is consistent with the stability of the catalyst during propane dehydrogenation at 680 ^{o}C.

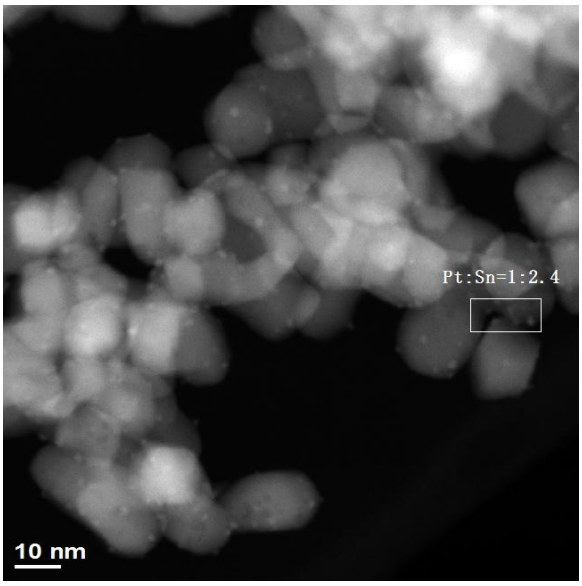

(a)

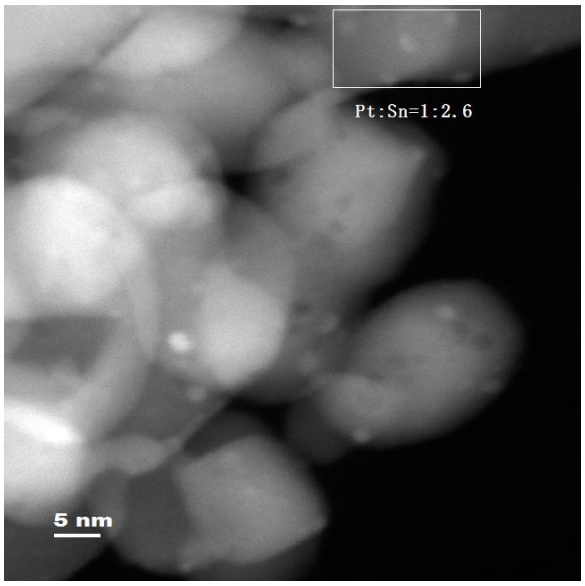

(b)

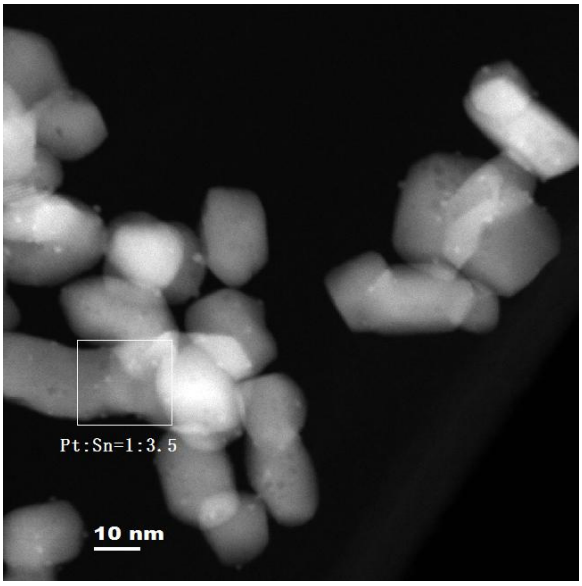

(c)

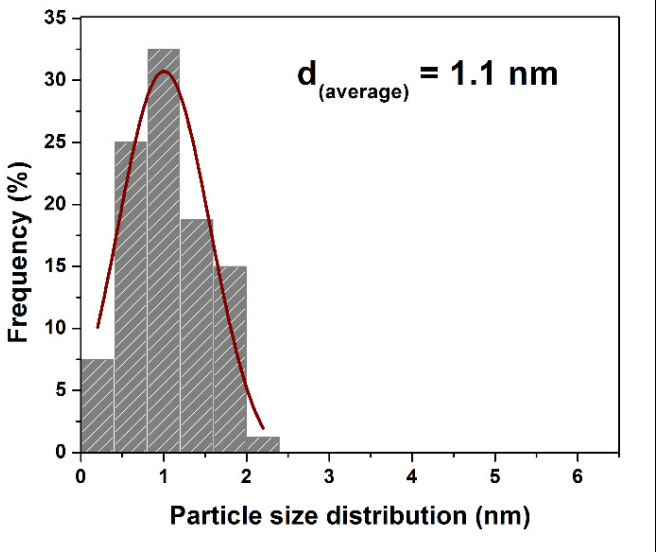

(d)

Supplementary Figure S11. (a-c)STEM-EDX analysis of spent Pt-Sn/CeO_2 catalyst after propane dehydrogenation at 680 °C showing the formation of sub-nm clusters having Pt/Sn atomic ratio around 1:3; (d) the particle size distribution of the spent Pt-Sn/CeO_2 catalyst after propane dehydrogenation at 680 °C. STEM-EDS analysis was performed from the regions of the samples as indicated in a-c. These boxed regions are larger than the size of the individual Pt-Snclusters because of limited signal from individual sub-nanometer particles. If STEM-EDS analysis of similar sized boxed regions is performed from areas without any visible clusters, we obtained negligible Pt and Sn signals. Therefore, the boxed regions provide an average Pt/Sn ratio for the clusters included in the box. These figures show that the Pt:Sn ratio in the spent catalyst is different from the Pt/Sn ratio in the fresh catalyst which is shown in the previous figures (Figure S7).

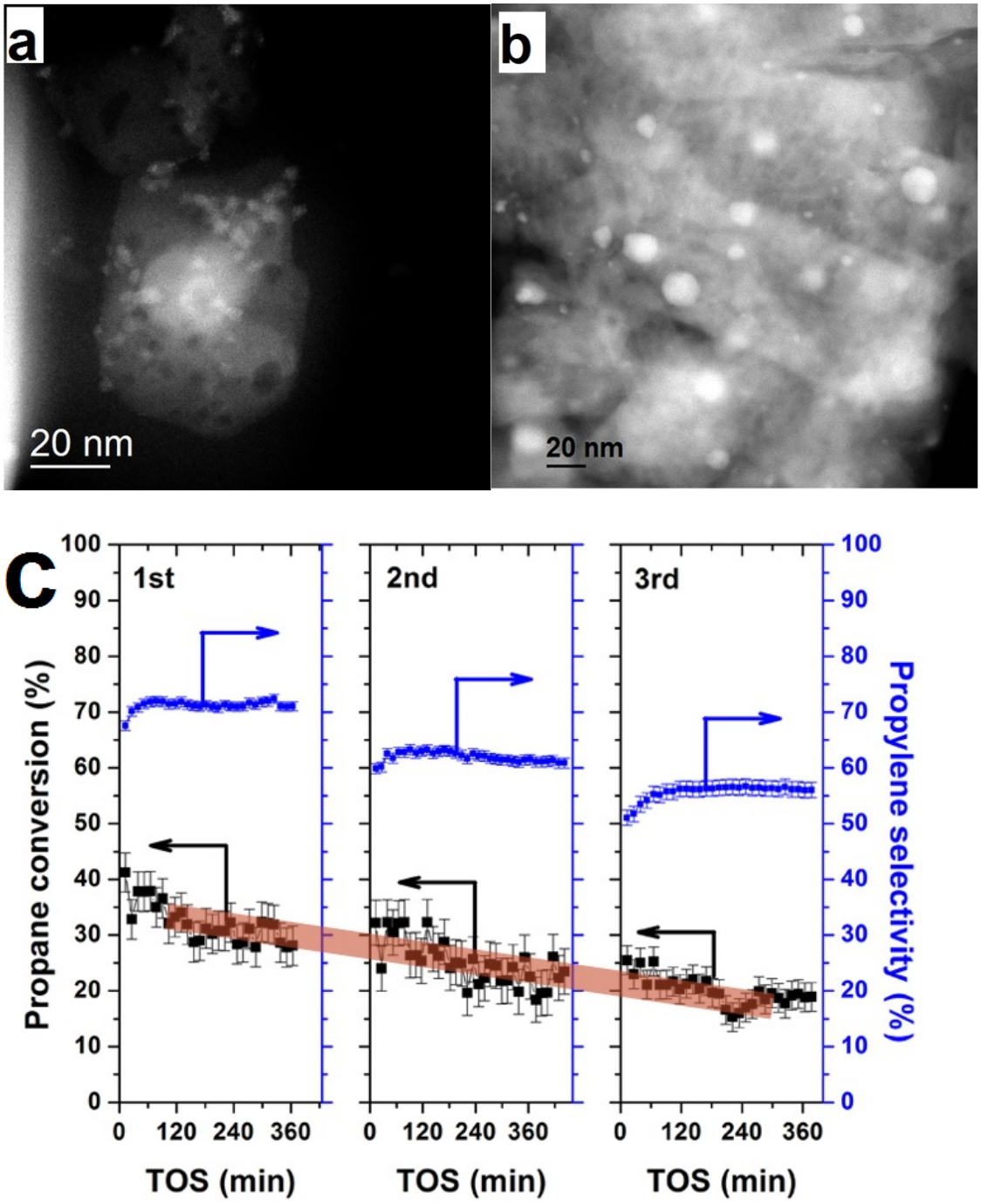

Supplementary Figure S12. (a) STEM image of Pt-Sn/Al_2O_3 catalyst in the as-prepared state. (b) STEM image of spent Pt-Sn/Al_2O_3 after 3 cycles of propane dehydrogenation at 680 °C with two intermediate oxidative regeneration cycles at 580 °C. (c) the propane dehydrogenation reactivity of Pt-Sn/Al_2O_3 measured at UNM showing a 6 h run, which was followed by oxidative treatment in flowing air at 580 °C (the error bars were calculated based on the standard deviation of the data). These data show a steady deactivation of the catalysts over time with negligible regeneration during the oxidative treatment. This behavior is very different from Pt-Sn/CeO_2 which is shown in Figure 2 in the main manuscript where we found complete regeneration and no deactivation.

Table S4

Carbon contents measured by CHN elemental analysis and by weight change during oxidation of the spent catalyst in the TGA. Each of the catalyst was used for propane dehydrogenation at 680 °C with the presence of water vapor at UNM.

Catalyst	Carbon content at end of 6h run at 680 °C (wt.%)	
	CHN elemental analysis [a]	TGA
Pt/CeO_2	0.3	0.9
$Pt\text{-}Sn/CeO_2$[b]	0.2	0.5
$Pt\text{-}Sn/Al_2O_3$	0.1	0.3

[a] Carbon concentrations were measured using a Costech ECS 4010 Elemental Analyzer coupled to a Thermo Finnigan Delta V Advantage Plus mass spectrometer via a CONFLO II interface. [b] The carbon contents on the $Pt\text{-}Sn/CeO_2$ catalyst after 1 h, 3 h and 5 h on stream are 0.1 wt.%, 0.3 wt.% and 0.2 wt.%, respectively, indicating the stability of the catalyst.

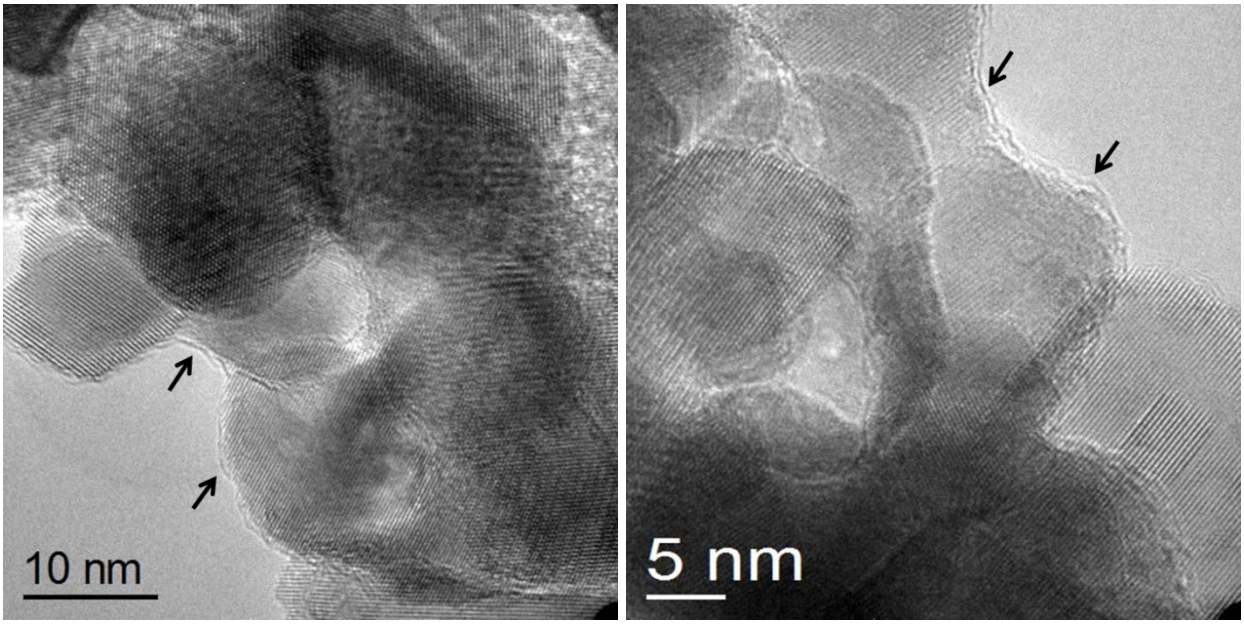

Supplementary Figure S13. TEM images of spent Pt-Sn/CeO_2 catalyst after propane dehydrogenation at 680 ºC for 6 h showing the formation of coke layers on the support surface (arrows).

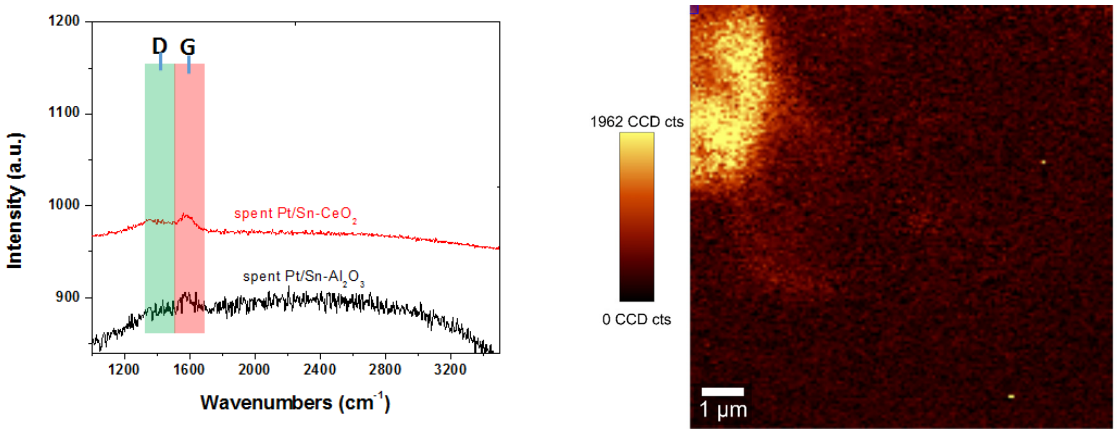

Supplementary Figure S14. Raman spectra of spent Pt-Sn/CeO_2 and Pt-Sn/Al_2O_3 catalyst and the large area Raman spectroscopy scan of Pt-Sn/CeO_2 catalyst after propane dehydrogenation at 680 ^oC for 6 h showing the formation of graphitic carbon on the supports.

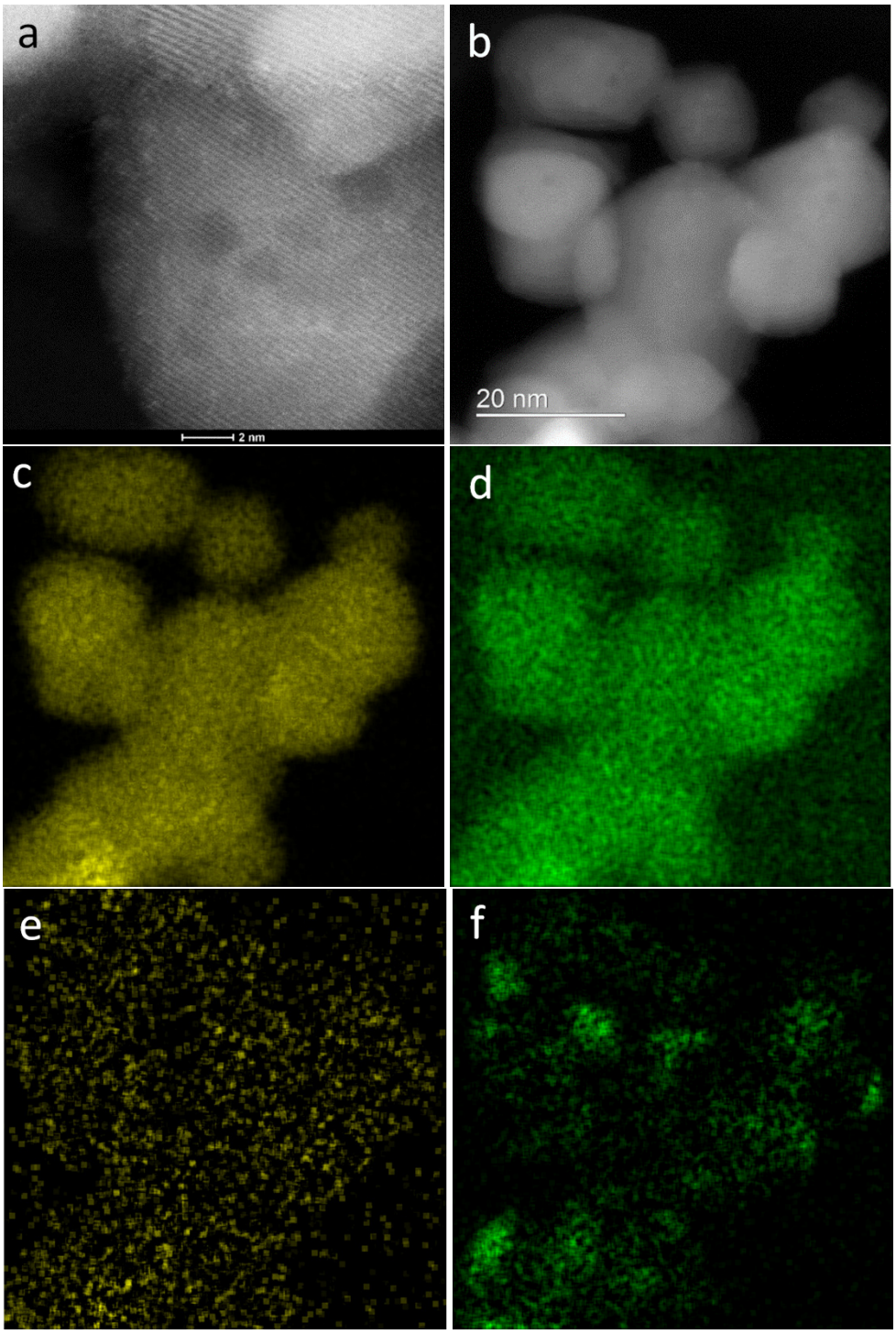

Supplementary Figure S15. STEM image and STEM-EDS mapping of the regenerated Pt-Sn/CeO_2 catalyst after calcining in air showing the locations of elements: (a) high magnification STEM image of spent Pt-Sn/CeO_2 regenerated at 580 ^oC in air showing the Pt species re-dispersed on the support for spent Pt-Sn/CeO_2 after regeneration; (b) low magnification STEM image of spent Pt-Sn/CeO_2 after regeneration; (c) STEM-EDS mapping showing the locations of cerium (Ce, yellow); (d) STEM-EDS mapping showing the locations of oxygen (O, green); (e) STEM-EDS mapping showing the locations of platinum (Pt, yellow); (f) STEM-EDS mapping showing the locations of tin

(Sn, green). This figure shows that regeneration by treatment in air at 580 °C causes the Pt to be atomically dispersed while the Sn remains in the form of nanoparticles.

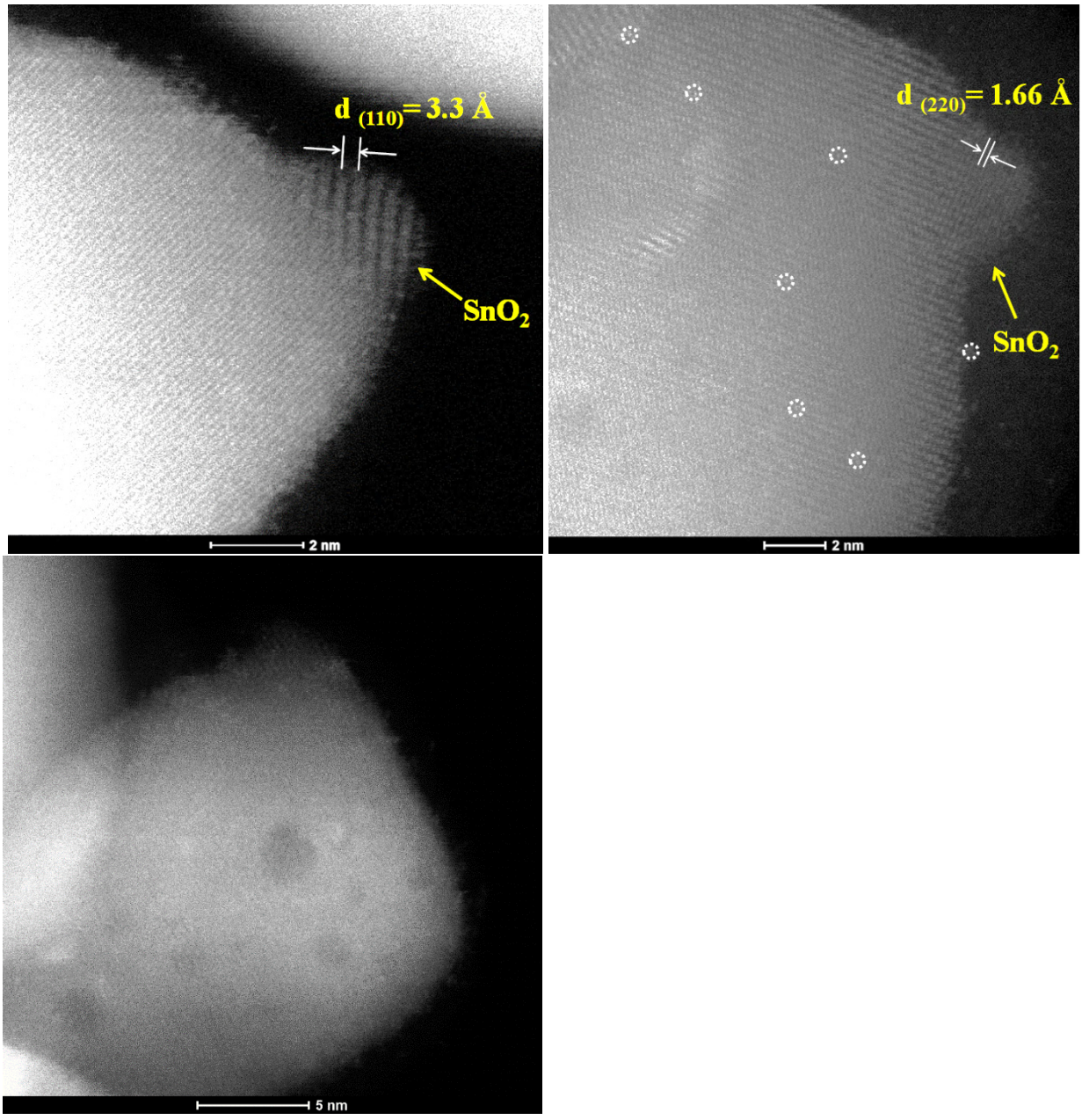

Supplementary Figure S16. STEM images of the spent Pt-Sn/CeO_2 catalyst after regenerating at 580 ºC for 2 h in air showing the Pt species were re-dispersed on the support and the existence of SnO_2 particles.

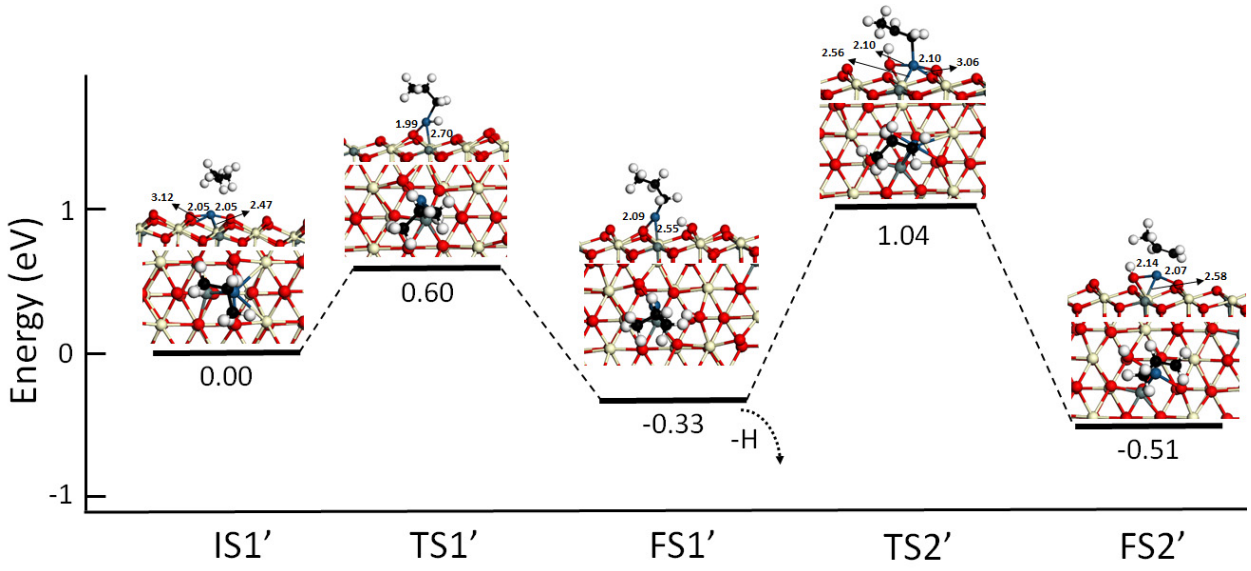

Supplementary Figure S17. The calculated reaction paths for $CH_3CH_2CH_3$* → $CH_3CH_2CH_2$* + H* and $CH_3CH_2CH_2$* → CH_3CHCH_2*+ H* on Pt-Sn/CeO_2.

Table S5. Propane dehydrogenation performance of severely sintered Pt-Sn catalysts.

Catalyst[a]	Conversion of Propane (%)	Propylene selectivity[b]	Carbon content at end of 6h run at 680 °C (wt.%)[c]
Pt-Sn/CeO_2	39.5	84.5	0.5
Pt-Sn(sintered)/CeO_2	12.6	71.6	0.1

[a] 0.1 g catalyst; 0.005 mL/min water; ambient pressure; reaction temperature: T=680 °C. [b] The weight loss of the spent catalyst was obtained from TGA carried out from 25 to 800 °C in the flowing air. [c] Pt-Sn(sintered)/CeO_2 was prepared by passing CH_4 over Pt-Sn/CeO_2 at 800 °C for 30 min, followed by calcination in flowing air at 500 °C for 1 h. The particle size increased to around 10 nm (Figure S19).

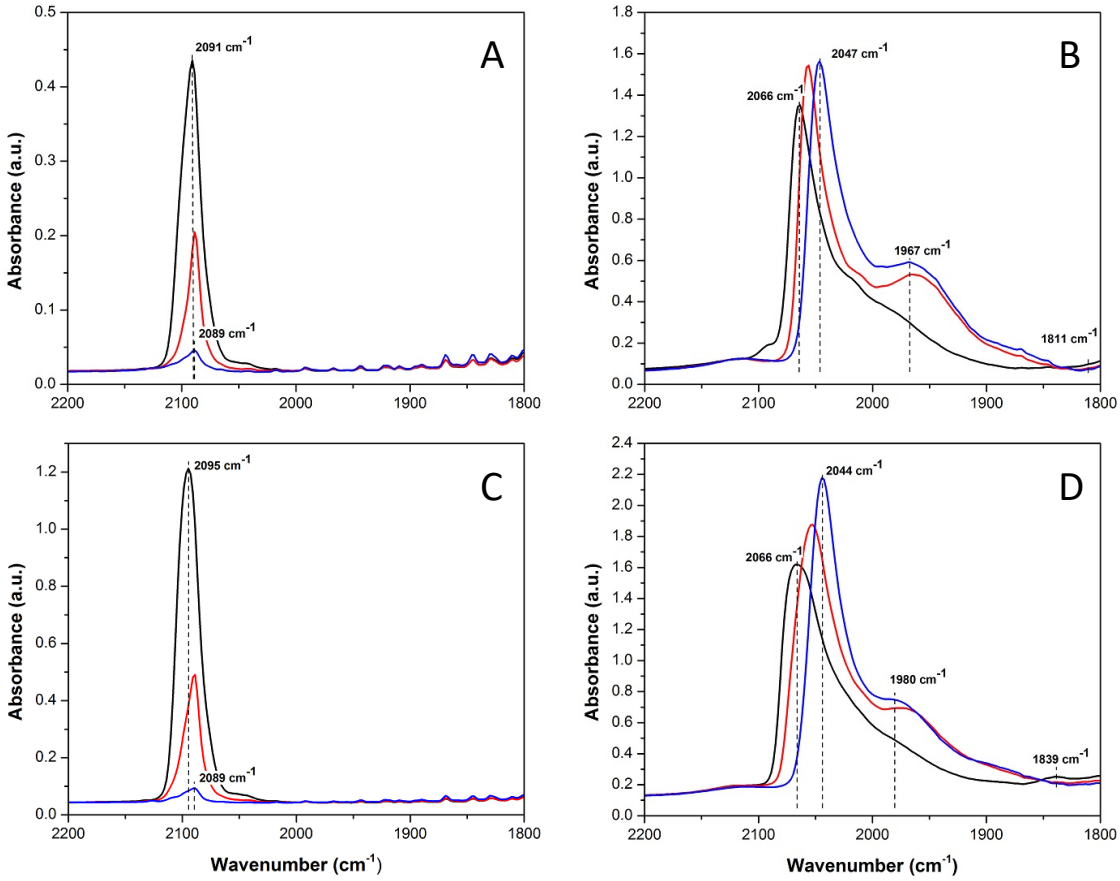

Supplementary Figure S18. CO-Temperature Programmed Desorption (TPD) experiments for catalysts (A) oxidized Pt/CeO_2, (B) reduced Pt/CeO_2 at 300 °C in H_2, (C) oxidized $Pt\text{-}Sn/CeO_2$ and (D) reduced $Pt\text{-}Sn/CeO_2$ at 300 °C in H_2. The FT-IR spectra during the CO TPD experiments were taken at 100 °C, 200 °C, and 300 °C and are shown in black, red, and blue, respectively. TPD using CO-DRIFTS for the oxidized Pt/CeO_2 (A) and $Pt\text{-}Sn/CeO_2$ (C) catalysts showed relatively similar CO peaks at 2091 and 2095 cm^{-1}, respectively. Upon desorption, the CO peak rapidly drops in intensity and shifts to 2089 cm^{-1} for both catalysts. The small degree of red shift upon desorption of the CO suggests that this band corresponds to isolated, oxidized Pt species on the ceria support. Such an assignment is consistent with the literature.[13] The AC-STEM results also show that the as-prepared catalyst consists of atomically dispersed Pt while XPS shows only oxidized Pt to be present on this sample. But we recognize that this band has also been assigned in the literature to CO adsorbed linearly on a Pt site adjacent to an oxidized Pt.[14] For the H_2 reduced samples, Pt/CeO_2 (B) and $Pt\text{-}Sn/CeO_2$ (D), both show a broad adsorption peak at 2066 cm^{-1} when recorded at 100 °C during TPD, which can be assigned to linearly adsorbed CO. Due to the broad nature of these peaks, the adsorbed CO cannot be selectively assigned to either step or terrace Pt sites, which can be both present. These peaks are redshifted when compared the oxidized samples A and C. This cause for these shifts could be related to either coverage affects or the presence of small, highly dispersed Pt clusters on the support. Heating during the CO TPD experiment to 300 °C, these peaks redshift to 2047 and 2044 cm^{-1} for the Pt/CeO_2 and $Pt\text{-}Sn/CeO_2$, respectively. Additionally, a new linearly absorbed CO peaks appears for both samples, 1967 cm^{-1} for Pt/CeO_2 and 1980 cm^{-1} for $Pt\text{-}Sn/CeO_2$. In addition, when comparing these spectra with those of the oxidized samples, minor contributions of bridged CO can be observed at around 1811 and 1839 cm^{-1} for respectively Pt/CeO_2 and $Pt\text{-}Sn/CeO_2$. In summary, the FTIR of adsorbed CO does not provide much information about the nature of the Pt in the Pt-Sn catalyst, which is also consistent with the literature [15].

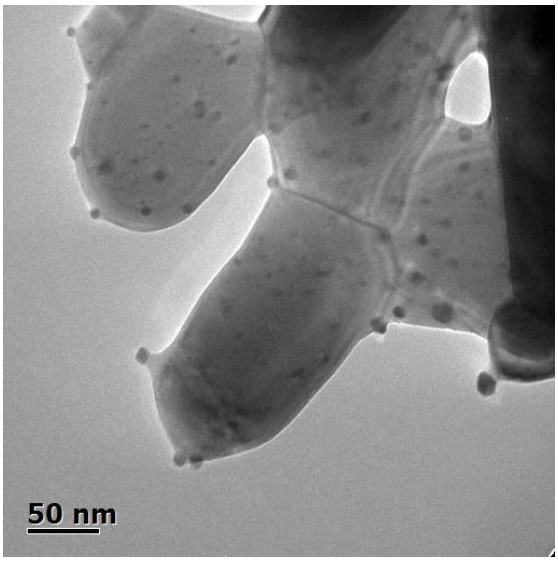

Supplementary Figure S19. TEM image of Pt-Sn (sintered)/CeO_2 catalyst; this catalyst was obtained by pretreating subnanometer Pt-Sn/CeO_2 in a flow of CH_4 at 800 ºC for 30 min. The carbon deposits were removed by calcining at 500 ºC in air for 1h. The particle size has grown to ca. 10 nm leading to lower reactivity for propane dehydrogenation.

References

1. Kresse G, Furthmuller J. Efficient iterative schemes for ab initio total-energy calculations using plane wave basis set. *Phys Rev B* 1996, **54:** 11169-11186.

2. Kresse G, Furthmuller J. Efficiency of ab initio total energy calculations for metals and semiconductors using plane wave basis set. *Comp Mater Sci* 1996, **6:** 15-50.

3. Perdew JP, Chevary JA, Vosko SH, Jackson KA, Pederson MR, Singh DJ*, et al.* Atoms, molecules, solids, and surfaces: Applications of the generalized gradient approximation for exchange and correlation. *Phys Rev B* 1992, **46:** 6671-6687.

4. Blöchl PE. Projector augmented-wave method. *Phys Rev B* 1994, **50:** 17953-17979.

5. McFarland EW, Metiu H. Catalysis by doped oxides. *Chem Rev* 2013, **113**(6)**:** 4391-4427.

6. Krcha MD, Janik MJ. Challenges in the use of density functional theory to examine catalysis by M-doped ceria surfaces. *Int J Quant Chem* 2014, **114**(1)**:** 8-13.

7. Duclos SJ, Vohra YK, Ruoff AL, Jayaraman A, Espinosa GP. High-pressure x-ray diffraction study of CeO_2 to 70 GPa and pressure-induced phase transformation from the fluorite structure. *Physical Review B* 1988, **38**(11)**:** 7755-7758.

8. Monkhorst HJ, Pack JD. Special points for Brillouin-zone integrations. *Phys Rev B* 1976, **13:** 5188-5192.

9. Henkelman G, Uberuaga BP, Jónsson H. A climbing image nudged elastic band method for finding saddle points and minimum energy paths. *J Chem Phys* 2000, **113:** 9901-9904.

10. Nykänen L, Honkala K. Density functional theory study on propane and propene adsorption on Pt(111) and PtSn alloy surfaces. *J Phys Chem C* 2011, **115**(19)**:** 9578-9586.

11. Yang M-L, Zhu Y-A, Zhou X-G, Sui Z-J, Chen D. First-principles calculations of propane dehydrogenation over PtSn catalysts. *ACS Catal* 2012, **2**(6)**:** 1247-1258.

12. Hauser AW, Gomes J, Bajdich M, Head-Gordon M, Bell AT. Subnanometer-sized Pt/Sn alloy cluster catalysts for the dehydrogenation of linear alkanes. *Phys Chem Chem Phys* 2013, **15**(47)**:** 20727-20734.

13. Qiao B, Wang A, Yang X, Allard LF, Jiang Z, Cui Y*, et al.* Single-atom catalysis of CO oxidation using Pt_1/FeO_x. *Nat Chem* 2011, **3**(8)**:** 634-641.

14. Jin T, Zhou Y, Mains GJ, White JM. Infrared and x-ray photoelectron spectroscopy study of carbon monoxide and carbon dioxide on platinum/ceria. *The Journal of Physical Chemistry* 1987, **91**(23)**:** 5931-5937.

15. Balakrishnan K, Schwank J. FTIR study of bimetallic Pt-Sn/Al_2O_3 catalysts. *Journal of Catalysis* 1992, **138**(2)**:** 491-499.